Interfacial Dzyaloshinskii-Moriya Interaction: Effect of 5d Band Filling and Correlation with Spin Mixing Conductance

Xin Ma, Guoqiang Yu, Chi Tang, Xiang Li, Congli He, Jing Shi, Kang L. Wang, and Xiaoqin Li

Phys. Rev. Lett. **120**, 157204 — Published 13 April 2018

DOI: 10.1103/PhysRevLett.120.157204

Interfacial Dzyaloshinskii–Moriya interaction: Effect of 5d band filling and correlation with spin mixing conductance

Xin Ma[1, 5, *], Guoqiang Yu[2, 6], Chi Tang[3], Xiang Li[2], Congli He[2], Jing Shi[3], Kang L. Wang[2, 4], and Xiaoqin Li[1]

[1]*Department of Physics, Center for Complex Quantum Systems, The University of Texas at Austin, Austin, Texas 78712, USA*
[2]*Department of Electrical Engineering, University of California, Los Angeles, California 90095, USA*
[3]*Department of Physics and Astronomy, University of California, Riverside, California 92521, USA*
[4]*Department of Physics, University of California, Los Angeles, California 90095, USA*
[5]*Department of Electrical and Computer Engineering, University of California, Santa Barbara, California 93106, USA*
[6]*Beijing National Laboratory for Condensed Matter Physics, Institute of Physics, Chinese Academy of Sciences, Beijing 100190, China*

The Dzyaloshinskii–Moriya Interaction (DMI) at the heavy metal (HM) and ferromagnetic metal (FM) interface has been recognized as a key ingredient in spintronic applications. Here we investigate the chemical trend of DMI on the $5d$ band filling ($5d^3$~$5d^{10}$) of the HM element in HM/FM (FM=CoFeB, Co)/MgO multilayer thin films. DMI is quantitatively evaluated by measuring asymmetric spin wave dispersion using Brillouin light scattering. Sign reversal and 20 times modification of the DMI coefficient D have been measured as the $5d$ HM element is varied. The chemical trend can be qualitatively understood by considering the $5d$ and $3d$ bands alignment at the HM/FM interface and the subsequent orbital hybridization around the Fermi level. Furthermore, a correlation is observed between DMI and effective spin mixing conductance at the HM/FM interfaces. Our results provide new insights into the interfacial DMI for designing future spintronic devices.

The Dzyaloshinskii-Moriya interaction (DMI) refers to a short-range antisymmetric exchange interaction that promotes chiral spin alignments in systems lacking space inversion symmetry [1, 2]. An interfacial DMI can be introduced in the ultrathin ferromagnetic metal (FM) layer adjacent to an anti-ferromagnetic [3] or heavy metal (HM) layer [4] possessing strong spin-orbit (SO) coupling. Such interfacial DMI has received significant attention recently, because its interplay with other SO effects provides a platform for exploring new phenomena promising for spintronic applications [5-10]. For instance, the DMI at FM/HM interfaces is essential to stabilize the Néel type spin configuration in magnetic skyrmions and domain walls with certain chirality [4]. In addition, the direction of skyrmion or domain wall motion driven by an electric current via SO torques is determined by the chirality of the spin texture, which in turn, is controlled by the sign of DMI [11-15]. In magnetization switching via SO torques, DMI presents an obstacle since an external magnetic field is required to overcome the chiral domain wall imposed by DMI [16].

The underlying physical principles that determine the DMI at HM/FM interfaces remains unclear despite many previous experimental and theoretical investigations. The DMI coefficient D is estimated on different multilayer structures by previous domain wall studies [17-19], where certain assumptions have to be applied. Direct measurement of D has been recently demonstrated with Brillouin light scattering (BLS) technique [20-29]. However, only a few isolated material systems have been investigated aiming to maximize D. So far, no systematic and direct experiment has been reported to investigate the chemical trend of DMI on the choice of material constituents of HM/FM bilayers. In addition, a number of theoretical and experimental studies have investigated the correlation between DMI and other SO effects including SO torques [30-32], proximity induced magnetization [33-35] and magnetic anisotropy [36]. In light of the important role played by SO interactions in DMI, systematic change of the HM element may be an effective route to seek DMI's correlation with other SO effects and to elucidate the underlying mechanisms of DMI at HM/FM interfaces.

In this letter, we investigate the impact of $5d$ band filling on DMI by systematically changing the $5d$ transition metal layer under the FM/MgO (FM=CoFeB, Co) thin film. A wide range variation of the $5d$ band filling ($5d^3$~$5d^{10}$) of the HM element leads to significant modification of D, which is evaluated quantitatively by measuring the asymmetric spin wave dispersion via Brillouin light scattering (BLS). Sign reversal of D is observed when the $5d$ band occupancy of the HM element changes from less than to more than half filled, similar to the Hund's rule. The strength of D exhibits systematic chemical trend and is maximized with the Pt underlayer, suggesting effective control of DMI by tuning the SO active $5d$ states near the Fermi level. A correlation between DMI and effective spin mixing conductance is observed by changing the HM layer. Such a correlation likely originates from the spin-flip processes between the $3d$ and $5d$ states that impact the DMI strength. In light of the recent success in controlling

DMI with multiple interfaces [24, 37, 38], our findings may further help design material structures with desired D for controlling skyrmions and chiral domain wall dynamics.

A series of X(5)/$Co_{20}Fe_{60}B_{20}$(1)/MgO(2)/Ta(2) and X(5)/ Co(1)/MgO(2)/Ta(2) (X = Ta, W, Ir, Pt) thin films were deposited by magnetron sputtering at room temperature on silicon substrates, where the numbers in parentheses denote the nominal layer thicknesses in nanometers. We used thermally oxidized Si substrates with around 100 nm SiO2 on surface, because the light signal is optimized for all incident angle used in BLS [39]. $Co_{20}Fe_{60}B_{20}$(1)/MgO(2)/ Ta(2) and Co(1)/MgO(2)/Ta(2) multilayers were also sputtered onto Au(5) underlayer prepared with e-beam evaporation. No further annealing procedure was applied after the deposition, in order to minimize the inter-diffusion of atoms between different layers [40]. As a result, the CoFeB, Co and HM layers are amorphous or polycrystalline. For those structures with X = W, Ir, and Pt, 5 nm-thick Ta seed layer was placed at the bottom of X HM underlayer to improve the HM/FM interface quality [27]. The HM layer thickness is chosen as 5 nm to saturate the DMI strength, excluding the variance of DMI introduced by HM thickness [23, 24]. We chose CoFeB as one candidate for the FM layer, considering its practical importance in existing spintronic applications [41, 42]. In view of the difficulty to theoretically investigate DMI in such alloyed systems, we further studied a series of control samples with Co as the FM layer to elucidate the physics.

BLS measurements were performed to investigate the frequency difference between counter-propagating Damon-Eshbach (DE) spin waves induced by DMI [3, 24]. Figure 1a shows the geometry of the BLS experiment, where an in-plane magnetic field **H** was applied along the z axis in all measurements. An s-polarized laser beam was incident on the sample, and the p-polarized component of the backscattered light was collected and sent to a Sandercock-type multipass tandem Fabry-Perot interferometer. In the light scattering process, the total momentum is conserved in the plane of the thin film. As a result, the Stokes (anti-Stokes) peaks in BLS spectra correspond to the creation (annihilation) of magnons with momentum $|k| = \frac{4\pi}{\lambda} sin\theta$ along $-x$ $(+x)$ direction as illustrated in Fig. 1a, where $\lambda = 532\,nm$ is the laser wavelength, and θ refers to the light incident angle.

Figure 1b displays typical BLS spectra for DE spin wave modes under opposite **H** directions on a representative sample Pt/CoFeB/MgO. The frequencies of the Stokes $(-k)$ and anti-Stokes (k) peaks are different, while the frequencies corresponding to $\pm k$ can be interchanged with each other by reversing the **H** direction. The spin wave frequency can be described by [3]

$$f = \frac{\gamma}{2\pi}\sqrt{\left(H + \frac{2A}{M_S}k^2 + 4\pi M_s\left(1-\xi(kt)\right) - \frac{2K_\perp}{M_s}\right)} * \sqrt{\left(H + \frac{2A}{M_S}k^2 + 4\pi M_s\xi(kt)\right)} - \varepsilon\left(K_\perp, k * \mathrm{sgn}(M_z)\right) - \mathrm{sgn}(M_z)\frac{\gamma}{\pi M_S}Dk \quad (1)$$

where H is the external field, γ is the gyromagnetic ratio, A is the exchange stiffness constant, M_S is the saturated magnetization, $\xi(kt) = 1 - (1 - e^{-|kt|})/|kt|$ with t being the CoFeB thickness, $K_\perp$ is the interfacial magnetic anisotropy which mainly originates from the CoFeB/MgO interface [25], and $\varepsilon(K_\perp, k)$ describes a correction in frequency due to interfacial anisotropy and non-reciprocity as discussed below. Both D and k can be positive or negative values in the formula. In Eq.1, the first term even in k on the right hand side describes the spin wave dispersion without DMI. The second term is much smaller than the DMI effect as discussed below. We take into account this second term explicitly in all analyses of DMI. Most importantly, the third term accounts for the frequency difference between counter-propagating spin waves induced by DMI and is odd in k.

To quantify the interfacial DMI constant D, momentum (k) resolved BLS measurements were performed through varying the incident angle. According to Eq. 1, we can simplify the determination of D by subtracting the BLS spectra.

$$\Delta f = \frac{\left(\left(f(-k,M_z) - f(k,M_z)\right) - \left(f(-k,-M_z) - f(k,-M_z)\right)\right)}{2} = \frac{2\gamma}{\pi M_S}Dk + \Delta\varepsilon(k) \quad (2)$$

where $\Delta\varepsilon(k) = \varepsilon(K_\perp, k) - \varepsilon(K_\perp, -k)$ is much smaller than the DMI term. In order to determine D accurately, we first estimated $\Delta\varepsilon(k)$ on different samples following previous studies [43]. $\Delta\varepsilon(k)$ originates from the non-reciprocity of DE spin waves in the presence of interfacial magnetic anisotropy $K_\perp$. In the DE geometry depicted in Fig.1a, spin waves propagating to $-x$ $(+x)$ direction localize near top CoFeB/MgO (bottom HM/CoFeB) interface, experience stronger (weaker) perpendicular anisotropy field $2K_\perp/M_S$ from CoFeB/MgO interface, and hence undergo a decrease (an increase) in the spin wave frequencies relatively. We first determine the $K_\perp$ values through the H dependence of spin wave frequency with $k = 0$ using normal incident light and fitting with Eq. 1, as shown in Fig. 2a. Then, the values of $K_\perp$ are used to estimate $\Delta\varepsilon(k)$ [44](see information for details [45]). Figure 2b plots the dependence of $\Delta\varepsilon(k)$ on k for different samples. After correcting Δf with $\Delta\varepsilon(k)$ in Eq.2, the slopes of the linear correlations can be used to determine the D values [47].

Figures 3a, 3b plot the measured frequency difference Δf as a function of k for the X/CoFeB/MgO (X = Ta, W, Ir, Pt, Au, MgO, and Pt/Cu(1)) multilayer thin films. The data is well fitted by a linear function in all cases as

described in Eq.2. Different slopes of the linear fittings on these samples mainly results from the change of D, because the magnitude of Δf is much larger than the $\Delta\varepsilon(k)$ in Fig. 2b. DMI is absent in the MgO/CoFeB/MgO thin film due to the recovery of inversion symmetry. Moreover, DMI strength drops significantly by inserting 1 nm Cu in between Pt and CoFeB layers [48]. No significant spin relaxation is expected in transversing the 1 nm Cu spacer between the Pt and CoFeB layers. The drastically reduced DMI results from disrupted hybridization between the $3d$ (CoFe) and $5d$ (Pt) orbitals as we elaborate below.

Our key finding in the chemical trend of DMI on $5d$ band filling of the HM element is summarized in Figs. 3c, 3d with $D_{\mathrm{S}} = D * t_{\mathrm{FM}}$, where similar trends are observed in the two sets of samples with CoFeB and Co as the FM layer [45]. Qualitative agreement between our results and previous first principle calculations [33, 49, 50] has been found with respect to the general chemical trend of DMI sign and magnitude, as discussed below. Quantitative agreement between theory and experiment is difficult to achieve, because a certain crystalline structure has to be assumed for HM and FM layers in theoretical models, differing from the amorphous or polycrystalline material structure used in our study and those in practical spintronic devices.

Evidently, the interfacial DMI reverses sign when the HM moves towards heavier element in Figs. 3c, 3d. The samples with Ta and W underlayers exhibit $D_{\mathrm{S}} > 0$ with right-handed magnetic chirality preferred, while those with Pt and Au underlayers have $D_{\mathrm{S}} < 0$ with left-handed magnetic chirality preferred. The sign of DMI is related to the $5d$ electron filling in the HM. Among the samples we investigated, the $5d$ bands of Ta and W are less than half filled by electrons, while those of Pt and Au are more than half filled. Such difference in $5d$ electron occupancy leads to opposite signs in the expectation value of SO coupling $< \mathbf{l} \cdot \mathbf{s} >$ between Ta (W) and Pt (Au) according to the Hund's rule. Originating from the SO coupling in the HM, the DMI sign should also be reversed between samples on Ta (W) and Pt (Au) underlayers, consistent with our observation in Figs. 3c, 3d. This interpretation agrees with related findings in B20 alloys [51] and a recent theoretical study that highlighted the important role of the Hund's rule in determining DMI at HM/FM interfaces [50]. We caution that the DMI signs are opposite between Ir/Co and Ir/CoFeB, and the same DMI sign between Ir/Co and Pt/Co agrees with previous report [26]. In literature, DMI constants with opposite signs have been reported experimentally at various Ir/FM interfaces of multilayer thin films (FM = Co, Ni, $(\mathrm{Ni/Co})_{\mathrm{N}}$, and CoFeB) [3, 19, 26, 52], and theoretical calculations also show that DMI changes sign between Ir/Co and Ir/Fe [50]. Because the $5d$ electron filling of Ir sits near the transition point of DMI sign reversal, the DMI sign becomes very sensitive to the $3d$ band alignment of the FM in Ir/FM multilayers.

The magnitude of DMI maximizes with Pt underlayer and decreases as the number of $5\,d$ electrons either increases or decreases in the HM element. In addition, there is a dramatic change (~ 20 times) in DMI strength between Ta and Pt and a sudden drop of the DMI strength from Pt to Au. This trend can be qualitatively understood by considering the $5d$ and $3d$ bands alignment at the HM/FM interface and the subsequent orbital hybridization around the Fermi level [50]. The increase of DMI strength from Ta to Pt is owing to the relocation of the Fermi level with respect to the $5d$ band of the HM. At different location (energy) of the broad $5d$ band, the $5d$ states are mainly with different orbital characters (i.e. $d_{xy}, d_{yz}, d_{xz}, d_{z^2}, d_{x^2-y^2}$) and hence contribute differently to DMI due to their varied degree of hybridization with $3d$ states [49]. By increasing the $5d$ electron number (i.e. Ta $5d^3$ to Pt $5d^9$), the Fermi level relocates towards the $5d$ states with certain orbital characters. Those $5\,d$ states around the Fermi level facilitate the spin-flip transitions between occupied and unoccupied $3\,d$ states, and hence dominantly contribute to the overall DMI [50]. The above qualitative arguments are supported by a first-principle calculation performed on a simple model system consisting of $5d$-$3d$ transition metal zigzag chains [49], where $5d_{xz}$ and $5d_{yz}$ states yield stronger contribution to the DMI and move towards the Fermi level with $5d^7 \sim 5d^9$ elelctrons in HM. Similarly, the sharp drop of DMI strength observed with Au layer originates from the absence of $5d$ states at the Fermi level and the subsequent reduction of $5\,d$-$3\,d$ orbital hybridization [33].

Finally, we report an observed correlation between DMI and spin pumping effect at HM/FM interfaces. As discussed above, the enhancement of DMI via $5\,d$-$3\,d$ hybridization is through facilitating the spin-flip transitions between $3d$ states that also involve transitions with $5d$ SO active states (i.e. $3\,d$-$5\,d$-$3\,d$ electron hopping). Such processes may also increase magnetic damping in the FM layer, because spin-flip transitions between $3d$ states make a significant contribution to magnetic damping in FM metals [45][53-56]. Therefore, one may expect a correlation between D_{S} and effective spin mixing conductance $g_{eff}^{\uparrow\downarrow}$ when changing the HM underlayer, as $g_{eff}^{\uparrow\downarrow}$ reflects the HM enhanced damping in FM α_{sp}. We determined the values of $g_{eff}^{\uparrow\downarrow}$ and α_{sp} through the full width half maximium (FWHM) of the BLS spectra [26][45]. Figures 4a, 4b (Figs. S4, S8) present the BLS linewidth FWHM as a function of H, which can be well fitted with $\mathrm{FWHM} = \frac{2\alpha\gamma}{\pi} H + \delta f_0$. Here, δf_0 is the extrinsic linewidth unrelated to H [57], and $\alpha = \alpha_{sp} + \alpha_0$. The intrinsic damping of CoFeB layer α_0 is estimated by measuring a sample with MgO underlayer in Fig. 4b, and we used $\alpha_0 = 0.011$ (bulk Co damping) for Co samples. The slopes of the linear dependence between FWHM and H as shown in Figs. 4a, 4b (Figs. S4, S8) are

used to determine α_{sp}. Furthermore, we determined effective spin mixing conductance using $g_{eff}^{\uparrow\downarrow} = \frac{4\pi M_S t_{FM}}{\gamma\hbar}\alpha_{sp}$ at different HM/FM interfaces. The estimated α_{sp} and $g_{eff}^{\uparrow\downarrow}$ on different samples (Tables S2, S3) agree well with the values found in the literature [58-63]. Figure 4c shows a correlation between D_S and $g_{eff}^{\uparrow\downarrow}$ by changing the HM layer at HM/FM interfaces. Both CoFeB and Co samples follow the same trend after we subtracted their intrinsic difference in damping when extracting α_{sp}. Finally, we report that both D and FWHM are inversely proportional to the CoFeB thickness t (Fig. 4d) in a representative Ir/CoFeB(wedge)/MgO sample, confirming that both the DMI and spin pumping effect originate from the HM/FM interface.

In conclusion, we investigate the dependence of the interfacial DMI on the $5d$ transition metal underlayer at HM/CoFeB/MgO multilayer thin films. The DMI coefficient changes by an order of magnitude and reverses sign when the HM moves towards heavier element in the $5\,d$ transition metal. The observations can be mostly explained by distinct degree of hybridization between $3d$ and $5d$ orbitals near the Fermi level owing to different $5d$ electron filling in the HM element. A correlation between DMI and effective spin mixing conductance, two interfacial effects at HM/FM interface, is observed, indicating the important role of spin-flip processes in DMI. Our results provide valuable guidance for designing magnetic multilayers with desired DMI value and chiral properties.

We gratefully acknowledge helpful discussions with Chun-Yeol You, Allan MacDonald, Pantelis Lapas, and Hua Chen. The collaboration among UT-Austin, UCLA and UCR are supported by SHINES, an Energy Frontier Research Center funded by the U.S. Department of Energy (DoE), Office of Science, Basic Energy Science (BES) under award # DE-SC0012670.

Email: * xma518@utexas.edu

[1] I. Dzyaloshinsky, Journal of Physics and Chemistry of Solids **4**, 241 (1958).

[2] T. Moriya, Physical Review Letters **4**, 228 (1960).

[3] X. Ma, G. Yu, S. A. Razavi, S. S. Sasaki, X. Li, K. Hao, S. H. Tolbert, K. L. Wang, and X. Li, Physical Review Letters **119**, 027202 (2017).

[4] A. Soumyanarayanan, N. Reyren, A. Fert, and C. Panagopoulos, Nature **539**, 509 (2016).

[5] W. Jiang, X. Zhang, G. Yu, W. Zhang, X. Wang, M. Benjamin Jungfleisch, J. E. Pearson, X. Cheng, O. Heinonen, K. L. Wang, Y. Zhou, A. Hoffmann, and S. G. E. te Velthuis, Nat Phys **13**, 162 (2017).

[6] K. Litzius, I. Lemesh, B. Kruger, P. Bassirian, L. Caretta, K. Richter, F. Buttner, K. Sato, O. A. Tretiakov, J. Forster, R. M. Reeve, M. Weigand, I. Bykova, H. Stoll, G. Schutz, G. S. D. Beach, and M. Klaui, Nat Phys **13**, 170 (2017).

[7] S. Woo, K. Litzius, B. Kruger, M.-Y. Im, L. Caretta, K. Richter, M. Mann, A. Krone, R. M. Reeve, M. Weigand, P. Agrawal, I. Lemesh, M.-A. Mawass, P. Fischer, M. Klaui, and G. S. D. Beach, Nat Mater **15**, 501 (2016).

[8] O. Boulle, J. Vogel, H. Yang, S. Pizzini, D. de Souza Chaves, A. Locatelli, T. O. Menteş, A. Sala, L. D. Buda-Prejbeanu, O. Klein, M. Belmeguenai, Y. Roussigné, A. Stashkevich, S. M. Chérif, L. Aballe, M. Foerster, M. Chshiev, S. Auffret, I. M. Miron, and G. Gaudin, Nat Nano **11**, 449 (2016).

[9] W. Jiang, P. Upadhyaya, W. Zhang, G. Yu, M. B. Jungfleisch, F. Y. Fradin, J. E. Pearson, Y. Tserkovnyak, K. L. Wang, O. Heinonen, S. G. E. te Velthuis, and A. Hoffmann, Science **349**, 283 (2015).

[10] W. Jiang, G. Chen, K. Liu, J. Zang, S. G. E. t. Velthuis, and A. Hoffmann, arXiv:1706.08295 (2017).

[11] K.-S. Ryu, L. Thomas, S.-H. Yang, and S. Parkin, Nat Nano **8**, 527 (2013).

[12] S. Emori, U. Bauer, S.-M. Ahn, E. Martinez, and G. S. D. Beach, Nat Mater **12**, 611 (2013).

[13] J. Iwasaki, M. Mochizuki, and N. Nagaosa, Nat Nano **8**, 742 (2013).

[14] A. Fert, V. Cros, and J. Sampaio, Nat Nano **8**, 152 (2013).

[15] T. Schulz, R. Ritz, A. Bauer, M. Halder, M. Wagner, C. Franz, C. Pfleiderer, K. Everschor, M. Garst, and A. Rosch, Nat Phys **8**, 301 (2012).

[16] O. J. Lee, L. Q. Liu, C. F. Pai, Y. Li, H. W. Tseng, P. G. Gowtham, J. P. Park, D. C. Ralph, and R. A. Buhrman, Physical Review B **89**, 024418 (2014).

[17] J. Torrejon, J. Kim, J. Sinha, S. Mitani, M. Hayashi, M. Yamanouchi, and H. Ohno, Nature Communications **5**, 4655 (2014).

[18] I. Gross, L. J. Martínez, J. P. Tetienne, T. Hingant, J. F. Roch, K. Garcia, R. Soucaille, J. P. Adam, J. V. Kim, S. Rohart, A. Thiaville, J. Torrejon, M. Hayashi, and V. Jacques, Physical Review B **94**, 064413 (2016).

[19] A. Hrabec, N. A. Porter, A. Wells, M. J. Benitez, G. Burnell, S. McVitie, D. McGrouther, T. A. Moore, and C. H. Marrows, Physical Review B **90**, 020402 (2014).

[20] H. T. Nembach, J. M. Shaw, M. Weiler, E. Jue, and T. J. Silva, Nat Phys **11**, 825 (2015).

[21] J. Cho, N.-H. Kim, S. Lee, J.-S. Kim, R. Lavrijsen, A. Solignac, Y. Yin, D.-S. Han, N. J. J. van Hoof, H. J. M. Swagten, B. Koopmans, and C.-Y. You, Nat Commun **6** (2015).

[22] K. Di, V. L. Zhang, H. S. Lim, S. C. Ng, M. H. Kuok, J. Yu, J. Yoon, X. Qiu, and H. Yang, Physical Review Letters **114**, 047201 (2015).

[23] S. Tacchi, R. E. Troncoso, M. Ahlberg, G. Gubbiotti, M. Madami, J. Åkerman, and P. Landeros, Physical Review Letters **118**, 147201 (2017).

[24] X. Ma, G. Yu, X. Li, T. Wang, D. Wu, K. S. Olsson, Z. Chu, K. An, J. Q. Xiao, K. L. Wang, and X. Li, Physical Review B **94**, 180408 (2016).

[25] A. K. Chaurasiya, C. Banerjee, S. Pan, S. Sahoo, S. Choudhury, J. Sinha, and A. Barman, Scientific reports **6**, 32592 (2016).

[26] N.-H. Kim, J. Jung, J. Cho, D.-S. Han, Y. Yin, J.-S. Kim, H. J. M. Swagten, and C.-Y. You, Applied Physics Letters **108**, 142406 (2016).

[27] N.-H. Kim, D.-S. Han, J. Jung, J. Cho, J.-S. Kim, H. J. M. Swagten, and C.-Y. You, Applied Physics Letters **107**, 142408 (2015).

[28] K. Di, V. L. Zhang, H. S. Lim, S. C. Ng, M. H. Kuok, X. Qiu, and H. Yang, Applied Physics Letters **106**, 052403 (2015).

[29] M. Belmeguenai, J.-P. Adam, Y. Roussigné, S. Eimer, T. Devolder, J.-V. Kim, S. M. Cherif, A. Stashkevich, and A. Thiaville, Physical Review B **91**, 180405 (2015).

[30] K.-W. Kim, H.-W. Lee, K.-J. Lee, and M. D. Stiles, Physical Review Letters **111**, 216601 (2013).

[31] J. Yu, X. Qiu, Y. Wu, J. Yoon, P. Deorani, J. M. Besbas, A. Manchon, and H. Yang, Scientific reports **6**, 32629 (2016).

[32] A. J. Berger, E. R. J. Edwards, H. T. Nembach, J. M. Shaw, A. D. Karenowska, M. Weiler, and T. J. Silva, arXiv:1611.05798 (2017).

[33] H. Yang, A. Thiaville, S. Rohart, A. Fert, and M. Chshiev, Physical Review Letters **115**, 267210 (2015).

[34] R. M. Rowan-Robinson, A. A. Stashkevich, Y. Roussigné, M. Belmeguenai, S. M. Chérif, A. Thiaville, T. P. A. Hase, A. T. Hindmarch, and D. Atkinson, Scientific Reports **7**, 16835 (2017).

[35] K.-S. Ryu, S.-H. Yang, L. Thomas, and S. S. P. Parkin, Nature Communications **5**, 3910 (2014).

[36] A. L. Balk, K. W. Kim, D. T. Pierce, M. D. Stiles, J. Unguris, and S. M. Stavis, Physical Review Letters **119**, 077205 (2017).

[37] C. Moreau-Luchaire, C. Moutafis, N. Reyren, J. Sampaio, C. A. F. Vaz, N. Van Horne, K. Bouzehouane, K. Garcia, C. Deranlot, P. Warnicke, P. Wohlhüter, J. M. George, M. Weigand, J. Raabe, V. Cros, and A. Fert, Nature Nanotechnology **11**, 444 (2016).

[38] A. Soumyanarayanan, M. Raju, A. L. Gonzalez Oyarce, A. K. C. Tan, M.-Y. Im, A. P. Petrović, P. Ho, K. H. Khoo, M. Tran, C. K. Gan, F. Ernult, and C. Panagopoulos, Nature Materials **16**, 898 (2017).

[39] A. Hrabec, M. Belmeguenai, A. Stashkevich, S. M. Chérif, S. Rohart, Y. Roussigné, and A. Thiaville, Applied Physics Letters **110**, 242402 (2017).

[40] A. W. J. Wells, P. M. Shepley, C. H. Marrows, and T. A. Moore, Physical Review B **95**, 054428 (2017).

[41] G. Yu, P. Upadhyaya, X. Li, W. Li, S. K. Kim, Y. Fan, K. L. Wong, Y. Tserkovnyak, P. K. Amiri, and K. L. Wang, Nano Letters **16**, 1981 (2016).

[42] S. Ikeda, K. Miura, H. Yamamoto, K. Mizunuma, H. D. Gan, M. Endo, S. Kanai, J. Hayakawa, F. Matsukura, and H. Ohno, Nat Mater **9**, 721 (2010).

[43] A. A. Stashkevich, M. Belmeguenai, Y. Roussigné, S. M. Cherif, M. Kostylev, M. Gabor, D. Lacour, C. Tiusan, and M. Hehn, Physical Review B **91**, 214409 (2015).

[44] O. Gladii, M. Haidar, Y. Henry, M. Kostylev, and M. Bailleul, Physical Review B **93**, 054430 (2016).

[45] See supplementary information for more BLS raw spectra, magnetic characterization results, determination of $\Delta\varepsilon(k)$, DMI measurements in HM/Co samples, magnetic field dependence of BLS linewidth in HM/CoFeB and HM/Co thin films, more discussion on the relation between DMI and effective spin mixing conductance, and more discussion on BLS FWHM which includes Ref [46].

[46] R. Arias and D. L. Mills, Physical Review B **60**, 7395 (1999).

[47] The DMI coefficient is determined with the Ms value obtained from Vibrating Sample Magnetometer (VSM) on each sample. The VSM results are shown in the supplemental material.

[48] N.-H. Kim, J. Cho, J. Jung, D.-S. Han, Y. Yin, J.-S. Kim, H. J. M. Swagten, K. Lee, M.-H. Jung, and C.-Y. You, AIP Advances **7**, 035213 (2017).

[49] V. Kashid, T. Schena, B. Zimmermann, Y. Mokrousov, S. Blügel, V. Shah, and H. G. Salunke, Physical Review B **90**, 054412 (2014).

[50] A. Belabbes, G. Bihlmayer, F. Bechstedt, S. Blügel, and A. Manchon, Physical Review Letters **117**, 247202 (2016).

[51] K. Shibata, X. Z. Yu, T. Hara, D. Morikawa, N. Kanazawa, K. Kimoto, S. Ishiwata, Y. Matsui, and Y. Tokura, Nature Nanotechnology **8**, 723 (2013).

[52] G. Chen, T. Ma, A. T. N'Diaye, H. Kwon, C. Won, Y. Wu, and A. K. Schmid, Nature Communications **4**, 2671 (2013).

[53] K. Gilmore, Y. U. Idzerda, and M. D. Stiles, Physical Review Letters **99**, 027204 (2007).

[54] P. He, X. Ma, J. W. Zhang, H. B. Zhao, G. Lüpke, Z. Shi, and S. M. Zhou, Physical Review Letters **110**, 077203 (2013).

[55] X. Ma, L. Ma, P. He, H. B. Zhao, S. M. Zhou, and G. Lüpke, Physical Review B **91**, 014438 (2015).

[56] Y. Liu, Z. Yuan, R. J. H. Wesselink, A. A. Starikov, and P. J. Kelly, Physical Review Letters **113**, 207202 (2014).

[57] The extrinsic linewidth mainly results from the instrument build-in linewidth from the interferometer and sample inhomogeneity.

[58] A. Conca, B. Heinz, M. R. Schweizer, S. Keller, E. T. Papaioannou, and B. Hillebrands, Physical Review B **95**, 174426 (2017).

[59] A. Ruiz-Calaforra, T. Brächer, V. Lauer, P. Pirro, B. Heinz, M. Geilen, A. V. Chumak, A. Conca, B. Leven, and B. Hillebrands, Journal of Applied Physics **117**, 163901 (2015).

[60] D.-J. Kim, S.-I. Kim, S.-Y. Park, K.-D. Lee, and B.-G. Park, Current Applied Physics **14**, 1344 (2014).

[61] C. He, A. Navabi, Q. Shao, G. Yu, D. Wu, W. Zhu, C. Zheng, X. Li, Q. L. He, S. A. Razavi, K. L. Wong, Z. Zhang, P. K. Amiri, and K. L. Wang, Applied Physics Letters **109**, 202404 (2016).

[62] S. Iihama, S. Mizukami, H. Naganuma, M. Oogane, Y. Ando, and T. Miyazaki, Physical Review B **89**, 174416 (2014).

[63] L. Liu, C.-F. Pai, Y. Li, H. W. Tseng, D. C. Ralph, and R. A. Buhrman, Science **336**, 555 (2012).

Figure 1:

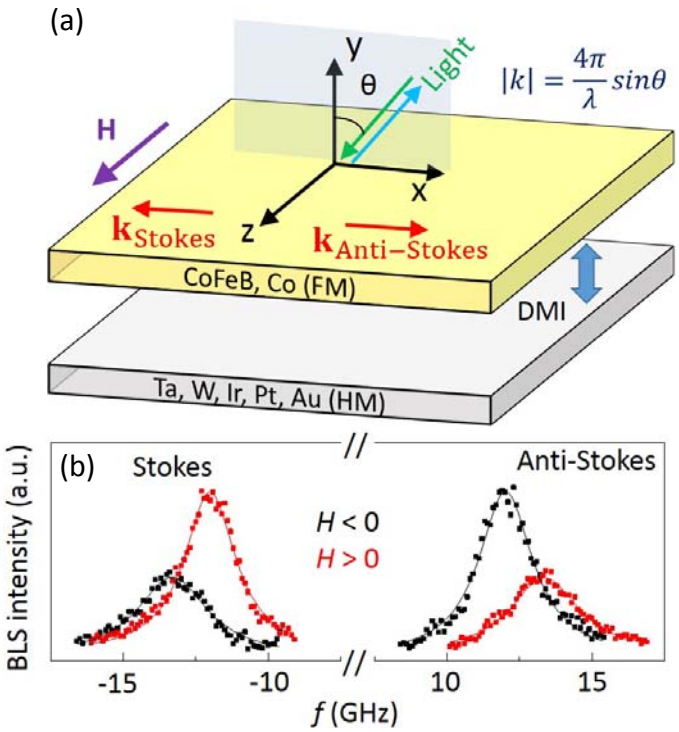

Fig. 1. (a) Schematics of BLS measurement geometry. (b) BLS spectra (with 100 MHz inter-channel frequency seperation) for DE spin waves recorded at a fixed incident angle $k = 13.9\ \mathrm{rad}/\mu\mathrm{m}$ under oppositely oriented external magnetic fields $\mathbf{H} = 2\ k\mathrm{Oe}$ in Pt/CoFeB/ MgO sample. The solid lines represent fittings with Lorentzian functions.

Figure 2

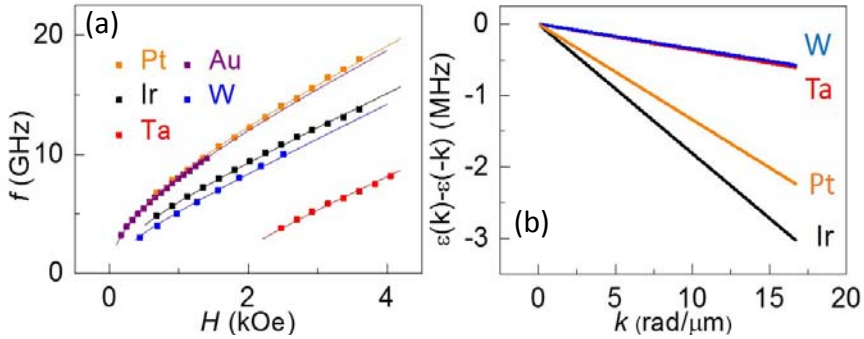

Fig. 2. (a) The dependence of spin wave frequency $f(k=0)$ on H in CoFeB samples with different underlayers. The solid lines are fittings with Eq.1 under $k=0$. (b) Simulation results of $\varepsilon(K_{\perp},k)-\varepsilon(K_{\perp},-k)$.

Figure 3:

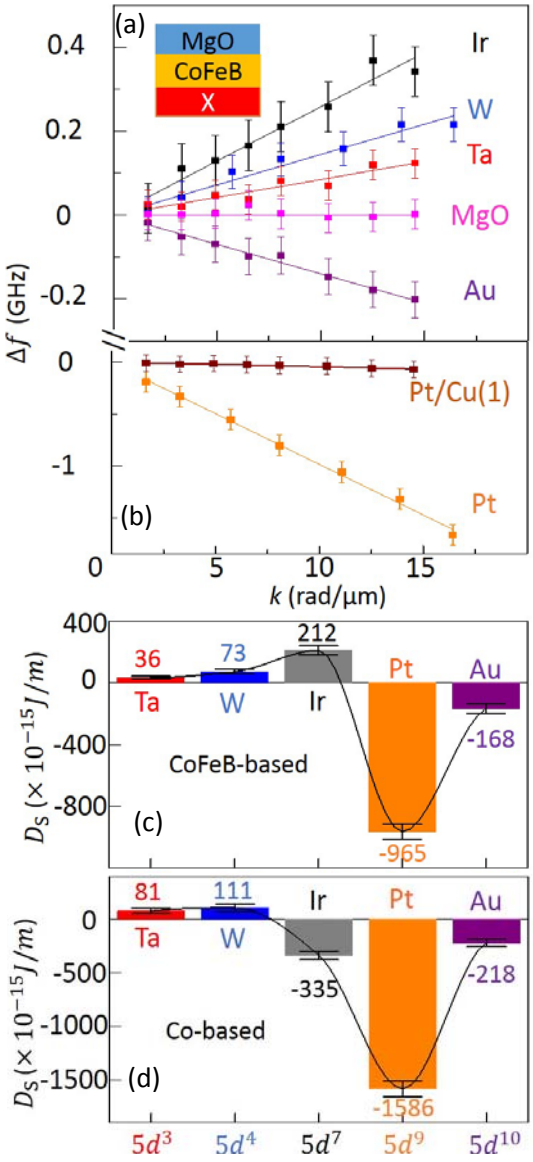

Fig. 3. (a, b) The linear dependence of Δf on k in CoFeB samples with different underlayers. (c, d) The D values determined at CoFeB and Co samples with different underlayers. The black lines serve as visual guides.

Figure 4:

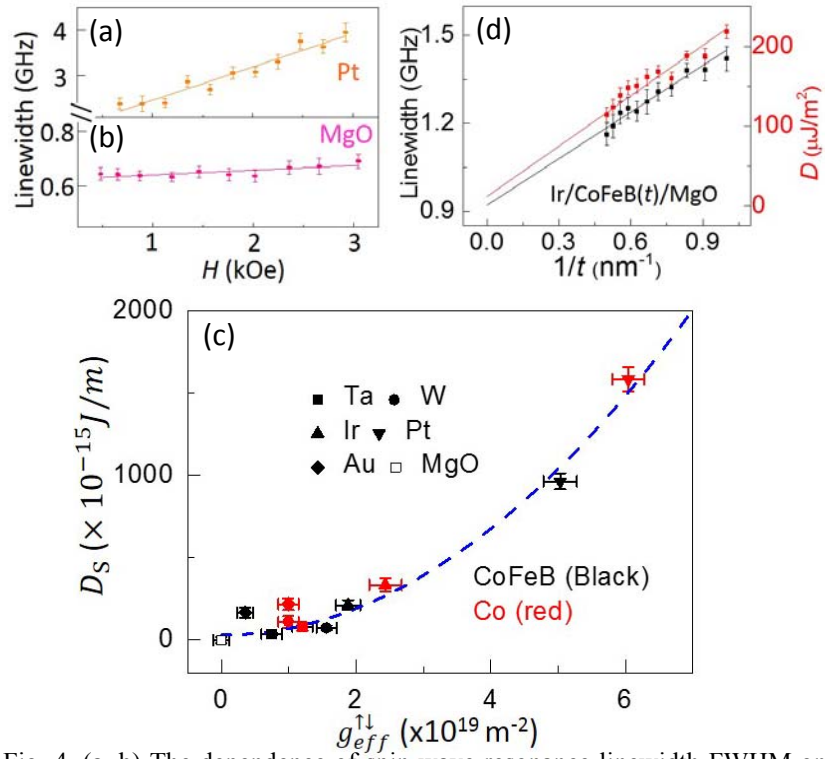

Fig. 4. (a, b) The dependence of spin wave resonance linewidth FWHM on H in CoFeB samples with different underlayers. (c) An observed correlation between D_S and $g_{eff}^{\uparrow\downarrow}$. The dashed line is a quadratic function for visual guide [45]. (d) The D (red) and linewidth FWHM (black) as a function of $1/t$(CoFeB) in Ir/CoFeB(wedge)/MgO sample at H=2 kOe. The solid lines are the least square fits.